CILAMCE 2017
Florianópolis - Santa Catarina - Brazil

COMPUTATIONAL MODELING OF CONCRETE WHEN SUBJECTED TO HIGH TEMPERATURES: APPLICATION OF A HYGROTHERMAL MODEL

Thaís Rossi Lopes Soares

Michèle Cristina Resende Farage

Flávia de Souza Bastos

thais.soares@engenharia.ufjf.br

michele.farage@ufjf.edu.br

flavia.bastos@gmail.com

Universidade Federal de Juiz de Fora

Rua José Lourenço Kelmer, S/n - Martelos, 36036-330, Juiz de Fora - MG, Brazil

Norbert Renault

norbert.renault@u-cergy.fr

Université de Cergy-Pontoise

5 Mail Gay-Lussac, Neuville-sur-Oise, 95031 Cergy-Pontoise cedex, France

Abstract. *High temperatures due to fire are amongst the most critical situations to which concrete may be exposed. For safety purposes, it is important to understand and preview the consequences of fire on the structural integrity of concrete. The mechanical degradation suffered by a concrete structure due to high temperatures is related to energy and mass transport in a porous medium. Hence, to describe a realistic behavior of concrete undergoing thermal loading, a model shall take into account simultaneously heat conduction, liquid and gaseous water flow, and the interactions of these fluid phases with the solid skeleton. Numerical simulations of the hygrothermal behavior of concrete specimen subjected to high temperature conditions are performed through a transient and nonlinear model, implemented in the Cast3M code which was developed at the French Atomic Research Center (CEA, France). In this study, we propose the application of a hygrothermal model to compare numerical and experimental results.*

Keywords: *Concrete, High temperature, Hygrothermal behavior*

1 INTRODUCTION

The use of concrete in construction presents many advantages in relation to other materials due to its mechanical performance, early strength increase, rheology of fresh concrete, durability and compactness. However, under certain situations where the concrete is exposed to high temperature (for example, caused by fires or by accidental situations in nuclear power plants), its behavior is very complex and influences the global behavior of a structure during heating, impacting on the safety of people. Therefore, it arises the necessity of studies related to this subject.

When undergoing thermal loads, there is an important risk of thermal instability of concrete, a phenomenon called spalling. Spalling happens when small scales fall out from the surface of the concrete, and the process is repeated as long as the required conditions are met; in progressive spalling, the element may also suddenly fail with a very large release of energy.

This paper carries a study about a model that allows the analyses of concrete hygrothermal behavior when subjected to high temperature loads: the temperature distribution, the modifications and the damage that the heating causes. The model used here was developed by the French Atomic Research Center (CEA, France) by Sercombe *et al.* (2001) and finished at L2MGC (Laboratoire de Mécanique et Matériaux du Génie Civil, Université de Cergy-Pontoise) by Morais *et al.* (2006a). The mathematical model was discretized and implemented in the Cast3M code, an open source software developed at CEA.

Morais *et al.* (2006b) validated the model proposed by Sercombe *et al.* (2001) using experimental results of a concrete whose formulation was proposed by Kanema *et al.* (2005). Morais *et al.* (2007) carried a comparison between two mechanical models inspired by Sercombe *et al.* (2001) model, that takes in account thermo-hydro-mechanical coupled effects in concrete. The common features of these models are that they can describe coupled water and temperature transfers through the porous medium and their interactions with the deformable solid matrix. Ferreira *et al.* (2014) presented the results of a hygrothermal model applied to a concrete-rock bilayer sample and employed experimental results to validate the model. At last Nguyen (2013), applied the hygrothermal model to large dimensions specimen and validated the numerical results using experimental data.

This work applies Sercombe *et al.* (2001) model in numerical studies based in experimental situations proposed by Mounajed & Obeid (2004), Mindeguia (2009) and Ranc *et al.* (2003). For each of these applications, the input data: such as geometry, concrete formulation, material parameters and constitutive equations is presented, followed by comparison between numerical and experimental results, and discussion.

2 CONCRETE UNDER FIRE CONDITIONS

Exposition to increasing temperatures may induce complicated phenomena in concrete, and predicting its behavior can become even more difficult due to its heterogeneity. Particularly, simply taking in account thermal properties is not enough to satisfactorily describe concrete behavior. Thus, it is necessary to consider fluid flow, energy exchange, and the hydration-dehydration phenomenon. Moreover, heating can also result in strong alterations in the concrete microstructure, and those may lead to modifications in its mechanical and transport properties.

Therefore, Dal Pont (2004) described the following phenomena observed at the cement paste when exposed to increasing temperature.

1. At the beginning of a fire, temperature rises on the heated surface. Free moisture, composed of liquid and vapor water, moves by diffusion toward the cold region of the concrete specimen.

2. When the temperature reaches $100°C$, water begins to boil, and the water vapor migrates to cold areas and condenses. Temperature increases is slowed until the boiling of water is complete in that region, as a result of the latent heat required for this phenomenon.

3. Meanwhile, the water vapor that condenses in the cold zone may affix itself to non-hydrated cement and cause new hydration. That process generates new calcium silicate hydrates (CSH), which makes mechanical properties of concrete better.

4. Temperature augmentation also causes dehydration. The chemical bounds that form CSH begin to be destroyed around $105°C$, thus converting hydrates products in anhydrous products and water, which vaporizes after absorbing heat. The dehydration process involves several hydrates products that form the concrete: as the temperature rises, more free water is generated and then vaporizes. The vaporization, being an endothermic reaction, influences the heating of the concrete, slowing down its progress.

5. After diffusion, free water tends to displace itself toward cold zones of concrete. Since this material has low permeability, liquid and vapor water do not penetrate quickly in the cold zones. Furthermore, the formation of water due to the dehydration phenomenon is faster than liquid-vapor water mix release. The combination of this two effects results in pore pressure increment, which may arrive to values with order of several atmospheres. It is also observed that the pressure peak moves toward cold areas of the concrete gradually increasing its value. There are studies, such as Mindeguia *et al.* (2010) and Morais *et al.* (2010), in which the increase in gas pressure in the pores is the basis of the phenomenon of spalling.

The spalling can be defined as the detachment of concrete fragments from the surface exposed to heating. According to Ferreira *et al.* (2014), it may seriously damage the integrity of the entire structure by direct exposure of structural steel to fire, increasing the risk of buckling under compression, the loss of the isolation property and other consequences. This phenomenon may be explained as the result of two mechanisms, as reported by Mindeguia *et al.* (2010):

- The thermo-mechanical process is characterized by high temperature gradients, principally in the first centimeters of the exposed surface. Mainly, those gradients are results of rapid heating, such as accidental fires, and lead to high compressive stresses near the exposed surface. Then, those stresses may locally exceed the concrete compressive strength and cause the ejection of pieces.

- The hygro-thermal process is associated with the movement of fluids in the porous medium, which may cause high pore pressure. Figure 1 shows the spalling mechanism related to water vapor pressure. When concrete is exposed to high temperatures, the water present in the pores as free or absorbed water begins to evaporate. Part of this water vapor migrates to inner and colder zones of the concrete, then begins to condense and progressively creates an obstruction of humidity ("moisture clog") near the exposed surface. The moisture clog is considered a region with high water content, which prevents fluid flow from heated to cold areas, hence increasing pore pressure. These pressures may locally exceed the concrete tensile strength and result in the occurrence of spalling.

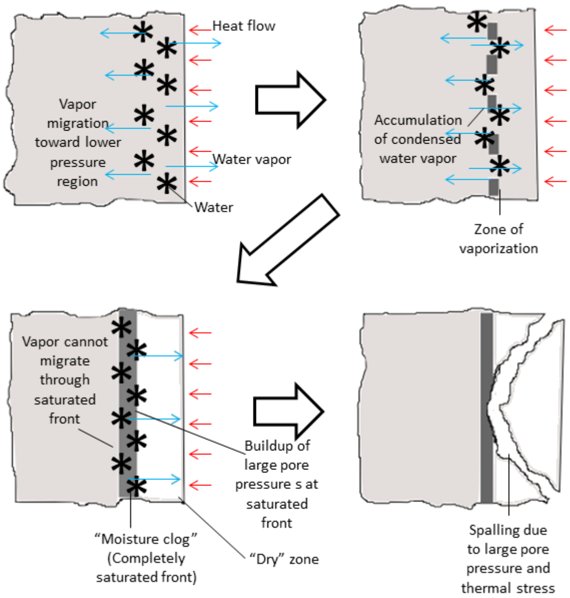

Figure 1: Spalling mechanism

3 EXPRESSION OF BALANCE EQUATIONS

In this section, the hygrothermal model proposed by Sercombe *et al.* (2001) in CEA, France and finished by Morais *et al.* (2006a) at L2MGC is presented.

3.1 General Assumptions

Some assumptions have been adopted to develop the coupled hygrothermal model for concrete behavior when subjected to high temperatures exposures. The main ones are:

1. The concrete is considered a porous, homogeneous, unsaturated and isotropic medium consisting of three phases: a solid skeleton composed of various chemical compounds and chemically bound water (index s), a liquid phase containing combined capillary and adsorbed water (index l), and a gas phase containing only water vapor (index v).

2. The system evolution is very slow. Therefore, the accelerations (second-order terms of the differential equations) will be disregarded, and the state of the porous medium will be considered to be quasi-static.

3. The phenomena of hysteresis from sorption curves is not considered. The relationship between saturation (S_l) and humidity (h_r) is $h_r = S_l$.

4. The hydric transformations in concrete are defined as two-phase changes:

   i The transformation of chemically bound water in liquid water, caused by dehydration of the solid phase.

   ii The transformation of liquid water in vapor.

5. The solid skeleton deformation is disregarded.
6. The transformations for the solid skeleton are considered to be infinitesimal.
7. The gas phase behaves as an ideal perfect gas.
8. The laws of heat conduction and mass flow are uncoupled.

3.2 Mass conservation equations

At high temperatures, the fluid mass balance must take in account on one hand, the quantities exchanged by vaporization/condensation and on the other hand the amount of liquid water freed by the solid phase dehydration. The mass conservation equations for liquid and vapor are:

$$\frac{\partial m_l}{\partial t} + \nabla.\vec{J}_l = \frac{\partial d}{\partial t} - \mu_{l\rightarrow v} \tag{1}$$

$$\frac{\partial m_v}{\partial t} + \nabla.\vec{J}_v = \mu_{l\rightarrow v} \tag{2}$$

where m_l and m_v are the liquid and vapor mass content per volume unit. These amounts are expressed in terms of the water degree of saturation (S_l) an the porosity (ϕ) by:

$$m_l = \rho_l \phi S_l \tag{3}$$

$$m_v = \rho_v \phi (1 - S_l) \tag{4}$$

In Eq. (3) and Eq. (4), $\rho_l(T)$ and $\rho_v(T, P_v)$ are respectively, the liquid and vapor water density, which are function of the temperature and water vapor pressure. In Eq. (1) and Eq. (2), $\mu_{l\rightarrow v}$ represents the rate of fluid mass change from liquid phase to gaseous phase. Lastly, d defines dehydration.

Darcy's law is written for each phase to define the flow $\vec{J}_i$, according to Eq. (5):

$$\vec{J}_i = -\rho_i \frac{K_i k_{ri}(S_l)}{\eta_l} \nabla(P_i), \tag{5}$$

where $i = l, v$ represent liquid or vapor flow, K_i the intrinsic permeability of each phase, k_{ri} the relative permeability of the phase, η_i the viscosity and P_i, the pressure.

In the modeling, it is assumed that there is a balance between liquid water and water vapor, and that those phases are separated by a curved interface. These phases being in thermodynamic equilibrium, the pressures of liquid water (P_l) and vapor (P_v) may be related by the Clapeyron equation.

$$P_l = P_{vs}(T) + \rho_l(T) \frac{RT}{M_v} ln \frac{P_v}{P_{vs}(T)} \tag{6}$$

where R represents the ideal gas constant, M_v is the molar mass of water vapor and P_{vs} is the water vapor saturation pressure.

Combining the mass conservation equations (Eq. (1) and Eq. (2)), the expression of flow given by Darcy's law (Eq. (5)) and Clapeyron equation (Eq. (6)), gives Eq. (7), which represents the water mechanisms:

$$\phi(\rho_l - \rho_v)\frac{\partial S_l}{\partial t} + \underbrace{\phi S_l \frac{\partial \rho_l}{\partial t}}_{\text{Term 2}} = \nabla \left[D_h\left(S_l, d, T\right) \vec{\nabla} S_l \right] + \frac{\partial d}{\partial t} \tag{7}$$

where D_h is the hydraulic conductivity, expressed as:

$$D_h\left(S_l, d, T\right) = \nabla.\left[\rho_l \frac{K_l k_{rl}(S_l)}{\eta_l} + \rho_v \frac{K_v k_{rv}(S_v)}{\eta_v}\right].P_{vs} \tag{8}$$

3.3 Energy balance equation

Associating the entropy conservation equation for a rigid porous medium, composed by three phases (solid, liquid and vapor) in local thermodynamic equilibrium, with the expression of heat flux given by Fourier's law, the equation of heat conservation is obtained (see Eq. (9)).

$$c\left(S_l, d\right) \frac{\partial T}{\partial t} = \nabla.\left(\lambda\left(T\right) \nabla T\right) - L_{l\to v}\left(T\right) \mu_{l\to v} + L_{s\to l} \frac{\partial d}{\partial t} \tag{9}$$

where L is the latent heat of phase change, $\mu_{l\to v}$ represents the rate of fluid mass change from liquid phase to gaseous phase, $\partial d/\partial t$ is the kinetics of dehydration and $c\left(S_l, d\right)$ is the volumetric heat capacity of concrete, that is given by Eq. (10):

$$c\left(S_l, d\right) = \rho_s C_s + \phi \rho_l\left(T\right) S_l C_l + \left(d_0 - d\right) C_u \tag{10}$$

where ρ_s and ρ_l are the densities of the solid part of concrete and of the liquid water; C_s, C_l and C_u are the specific heat capacity of solid part, free water and chemically bound water, respectively; and d_0 and d are the initial mass of chemically bound water and the mass of water generated by dehydration, respectively.

4 TIME DISCRETIZATION

The differential equations Eq. (7) and Eq. (9) form a system of two equations and two unknows, temperature (T) and liquid saturation (S_l), which describes the coupled phenomena of heat and humidity transfer.

$$\begin{cases} \phi(\rho_l - \rho_v)\frac{\partial S_l}{\partial t} + \underbrace{\phi S_l \frac{\partial \rho_l}{\partial t}}_{\text{Term 2}} = \nabla\left[D_h\left(S_l, d, T\right)\vec{\nabla} S_l\right] + \frac{\partial d}{\partial t} \\ c\left(S_l, d\right)\frac{\partial T}{\partial t} = \nabla.\left(\lambda\left(T\right)\nabla T\right) - L_{l\to v}\left(T\right)\mu_{l\to v} + L_{s\to l}\frac{\partial d}{\partial t} \end{cases} \tag{11}$$

After using finite difference method for temporal discretization, the system may be reorganized in a form where it is possible to observe that both equations have similar structures:

$$\begin{cases} \phi((\rho_l)_{i+1} - (\rho_v)_{i+1} + (\rho_l)_{i+1} - (\rho_l)_i)\frac{\partial S_l}{\partial t} - \underbrace{\nabla\left[D_h\left(S_l, d, T\right)\vec{\nabla} S_l\right]}_{\text{Diffusion}} = \underbrace{\frac{\partial d}{\partial t} - [(\rho_l)_{i+1} - (\rho_l)_i].\phi.\frac{(S_l)_i}{\Delta t}}_{\text{Source}} \\ c\left(S_l, d\right)\frac{\partial T}{\partial t} - \underbrace{\nabla.\left(\lambda\left(T\right)\nabla T\right)}_{\text{Diffusion}} = \underbrace{-L_{l\to v}\left(T\right)\mu_{l\to v} + L_{s\to l}\frac{\partial d}{\partial t}}_{\text{Source}} \end{cases} \tag{12}$$

If necessary, to better understand the mathematical modeling, one can consult Soares *et al.* (2017), where the equations development are presented in more detail.

The final system presented in Eq. (12) is implemented in Cast3M, an open source code developed by the French Atomic Research Center (CEA) in France. The solver enables the user to resolve partial differential equations through the finite element method. So, the user can adapt and incorporate models on it. The language employed is based on object-oriented programming and named GIBIANE, and the objects are created using pre-defined operators.

In this work, the equations were implemented in GIBIANE and were treated separately. In the procedure that solves them, it is possible to adopt an explicit or implicit resolution by the theta method.

5 MATERIAL PARAMETERS AND CONSTITUTIVE EQUATIONS

In this section, the evolutions of different material parameters and functions, such as quantity of water generated by dehydration, porosity, intrinsic and relative permeability, thermal capacity and conductivity for the solid skeleton, and enthalpy of vaporization and dehydration, are defined regarding temperature and liquid saturation. They are expressed in Table 1 and Table 2, where m_c and m_g are the mass of cement and granulate, respectively.

Table 1: Evolution of model parameters in function of temperature or liquid saturation $(T \ \ in \ \ °C)$.

Data	Value	Auxiliary parameters	Unit
Liquid water density	$\rho_l = 314.4 + 685.6\left[1-\left(\frac{T}{374.14}\right)^{\frac{1}{0.55}}\right]^{0.55}$	-	kg/m^3
Vapor water density	$\rho_v = \frac{P_{vs}M_v}{R\,(T+273.15)}$	$R = 8.314(J/mol/K)$ $M_v = 0.018(kg/mol)$	kg/m^3
Liquid water viscosity	$\eta_l = 2.414\times10^{-5}\times e^{\frac{570.58058}{T+133.15}}$	-	$kg/m/s$
Vapor water viscosity	$\eta_v = (3.85\times10^{-8}\times T)+10^{-5}$	-	$kg/m/s$
Liquid intrinsic permeability	$K_l = K_{l0}\times e^{0.126d}$	$K_{l0} = 3.5\times10^{-19}$	m^2
Vapor water intrinsic permeability	$K_v = K_{v0}\times e^{0.126d}$	$K_{v0} = 3.5\times10^{-16}$	m^2
Liquid relative permeability	$k_{rl}(S_l) = \sqrt{S_l}\times\left[1-\left(1-S_l^{1/m}\right)^m\right]^2$	$m = 0.5$	-
Vapor relative permeability	$k_{rv}(S_l) = \sqrt{1-S_l}\times[1-(1-S_l)^m]^{2m}$	$m = 0.5$	-
Vapor saturation pressure	$P_{vs} = P_0\times exp\left[\frac{40500}{R}\left(\frac{T-100}{373.15(T+273.15)}\right)\right]$	$R = 8.314(J/mol/K)$ $P_0 = 101325(Pa)$	Pa
Thermal conductivity	$\lambda = 1.36-0.136\left(\frac{T}{100}\right)+0.0057\left(\frac{T}{100}\right)^2$	-	W/mK
Dehydration latent heat	$L_{s\to l}2500\times10^3$	-	(kJ/kg)
Vaporization latent heat	$L_{l\to v} = \frac{2450.2502-6.433949\times T}{1-0.0019057413\times T-7.0023846\times10^{-7}\times T^2}$	-	(kJ/kg)
Qty. of dehydrated water	$d = 0,136\,(T-60)\ \ para\ \ T>60$	-	kg/m^3
Porosity	$\phi(d) = \phi_0+\frac{d}{\rho_{hid}}$	-	-

6 NUMERICAL ANALYSIS

In this section, three applications are proposed. For each case, a section in which the relevant data, results, and discussion will be presented.

Table 2: Specific heat

Specific heat	$(J/kg°C)$
Cement (C_c)	750
Aggregate (C_g)	800
Free water (C_l)	4184
Bound water (C_u)	3760
Solid phase (C_s)	$\frac{C_c m_c + C_g m_g}{m_c + m_g}$

6.1 Experiment 1: Mounajed & Obeid (2004)

In Mounajed & Obeid (2004), the authors proposed the development of a thermal-hydro-mechanical coupling model (THM) that simulates the behavior of concrete at high temperatures, and later experimental results were used to validate the suggested model. Here, the data from the Numerical Simulation section is used to try to replicate the experimental results.

The simulation consists of applying a thermal load on the upper face of concrete samples having a prismatic shape ($30 \times 30 \times 12\ cm^3$), whereas four lateral faces are surrounded with a heat insulation material. This configuration leads to unidirectional thermal load conditions, therefore the numerical simulation will be made on an oblong section of a unit width and of a length of $12cm$, as illustrated in Fig. 2.

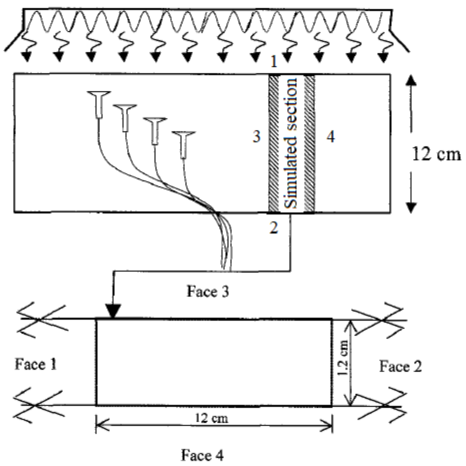

Figure 2: Geometry schema

A normal strength concrete M30 is subjected to temperature load up to $600°C$ in $6\ h$. As the article does not introduce the concrete formulation, just its type, the values used in this work are generic ones, that are shown in Table3.

The guidelines to the implantation are:

- **Face 1** is exposed to the thermal load.
  - Fixed gas pressure equals to the atmospheric pressure (101325 Pa).

Table 3: M30 - Concrete formulation

Constituent	(kg/m^3)
Cement	400
Aggregate	1950
Mix water	177

  - Fixed relative humidity equals to 0.05%.
  - Ambient temperature equals to $600°C$.
- **Face 2** is in direct contact with the external environment defined by an ambient temperature of $25°C$ and a relative humidity equal to 65%.
  - Fixed gas pressure equals to the atmospheric pressure (101325 Pa).
- **Faces 3 and 4** are symmetry surfaces. They correspond to the surfaces parallel to the lateral faces of the test samples. The distance between these two surfaces is chosen for the model equal to $1.2cm$; this value is arbitrary as it does not influence the results because of the unidirectional nature of the flow.
  - Null flux due to the symmetry condition.

The initial conditions used are illustrated in Table 4.

Table 4: Initial conditions

Data	value	Unity
Temperature	25	$°C$
Porosity	0.10	-
Intrinsic permeability	10^{-17}	m^2
Thermal conductivity	2.0	W/mK

Once all the data was inserted in the Cast3M code, the algorithm was executed without success, right in the first time step, problems to calculate the liquid relative permeability arises. After doing some tests, it was concluded that the really small relative humidity condition in Face 1 ($Hr = 0.005$) caused numerical issues. As the objective was to compare experimental and numerical results, it was not ideal to change this value. Therefore, this application was discarded.

6.2 Experiment 2: Ranc *et al.* (2003)

Ranc *et al.* (2003) presented the analysis of experimental data obtained on a reinforced concrete prototype of a storage structure for nuclear waste heated on one face at $0.1°C$ until $200°C$. The temperature, the water vapor pressure and internal humidity within the thickness of the structure were continuously monitored. In this section, these results will be compared to numerical results of the simulated model. The structure simulated is presented in Fig. 3. Since it has a cylindrical structure, the axisymmetric option was used in the calculations and the geometry utilized was the face of a half of the specimen.

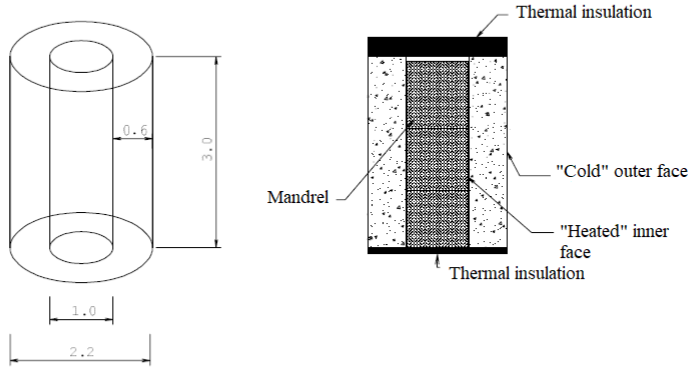

Figure 3: Schematic representation of the model and boundary conditions

A particularity of this experiment is that there was a power outage during the heating, and therefore the load curve, has the following shape, as shown in Fig. 4.

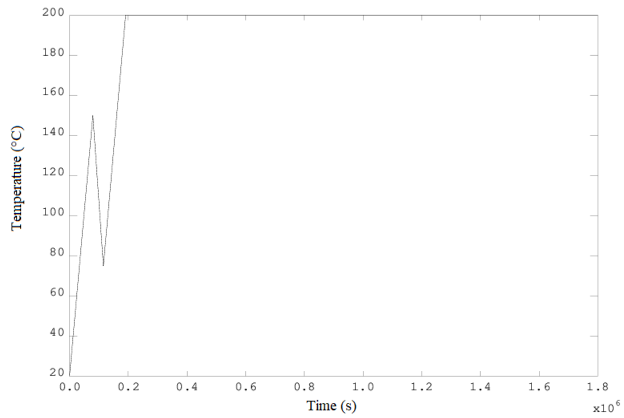

Figure 4: Heating cycle imposed on the internal wall of the model

The material utilized is a high performance concrete (compressive strength $60MPa$), its formulation is illustrated in Table5.

Table 5: Concrete formulation

Constituent	(kg/m^3)
Cement	354
Aggregate	1877
Mix water	154

The initial conditions used, are illustrated in Table 6.

Table 6: Initial conditions

Data	value	Unity
Temperature	20	$°C$
Saturation	0.97	-
Porosity	0.10	-
Intrinsic permeability	10^{-17}	m^2
Thermal conductivity	2.2	W/mK

When the algorithm was executed, the first time step was concluded without problems, but at the second one, there were numerical problems in the computation of the liquid water density due to the temperature field. That implied in the fact that the model is sensible to cooling situation, besides that, the load application, with the heating in the inner wall and constant ambient temperature in the outer face, may require another boundary conditions, such as convection, aside from the ones used here. Which may have caused the numerical errors.

6.3 Experiment 3: Mindeguia (2009)

In Mindeguia (2009), the author proposed a study about the spalling phenomenon of concrete. Hence an experimental study using an ordinary concrete (compressive strength $40MPa$) and a high performance concrete (compressive strength $60MPa$) is made. The evolution with temperature of several properties, such as gas permeability, water porosity, and thermal properties, have been assessed. Besides that, the temperature and gas pressure evolution were measured.

In this work, the simulations of an ordinary ($B40$) and a high performance ($B60$) concrete cylindrical specimen ($\phi\ 160 \times h\ 320\ mm$) in conditions similar to the experiment were made to compare its results with the experimental ones.

Since it is a cylindrical structure, the axisymmetric option was used in the calculations and the geometry utilized was the face of a quarter of the specimen, as Fig. 5 shows.

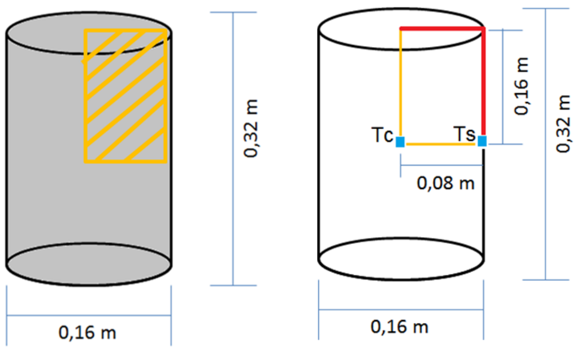

Figure 5: Specimen schema

A thermal load was applied in the form of temperature increase at the external geometry sides (in red in Fig. 5). The initial temperature of the domain was $20°C$, the velocity of heating was $1°C/min$ and the final temperature was $600°C$. Accordingly to the symmetry condition, the inner sides (in yellow in Fig. 5) had null flux. The concrete formulations used are presented at Table 7.

Table 7: B40 and B60 - Concrete formulation

(a) B40

Constituent	(kg/m^3)
Cement	350
Aggregate	1895
Mix water	188

(b) B60

Constituent	(kg/m^3)
Cement	550
Aggregate	1895
Mix water	165

In this application, experimental values of porosity and thermal conductivity are used to interpolate these properties curves, instead of using the evolutions suggested in Table 1. The experimental data for porosity and thermal conductivity is shown in Table 8. The initial conditions used are illustrated in Table 9.

Table 8: B40 and B60 - Porosity and Thermal conductivity

(a) Porosity

Porosity	$20°C$	$80°C$	$120°C$	$250°C$	$400°C$
B40	13.85%	13.85%	13.00%	14.30%	15.95%
B60	10.55%	10.55%	11.50%	13.15%	14.05%

(b) Thermal conductivity

Thermal conductivity (W/mK)	$20°C$	$150°C$	$300°C$	$600°C$
B40	2.55	1.97	1.45	1.21
B60	2.42	1.81	1.38	0.89

Table 9: B40 and B60 - Initial conditions

(a) B40

Data	value	Unity
Temperature	20	$^{\circ}C$
Saturation	0.48	-
Porosity	0.1385	-
Intrinsic permeability	5.53×10^{-16}	m^2
Thermal conductivity	2.55	W/mK

(b) B60

Data	value	Unity
Temperature	20	$^{\circ}C$
Saturation	0.48	-
Porosity	0.1055	-
Intrinsic permeability	1.67×10^{-16}	m^2
Thermal conductivity	2.42	W/mK

The code was executed and its results compared to experimental data relative to the points illustrated in Fig. 6. The temperature results are shown in Fig. 7 and Fig. 8. For both concrete formulations, $B40$ and $B60$, it is possible to observe that the curve obtained numerically follow the experimental data evolution. There are, however, regions where the results vary more. These perturbations are justified by the change of heating rate due to the latent heat necessary to vaporization.

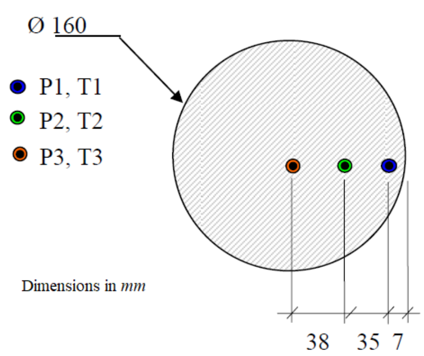

Figure 6: Layout of the distribution of probes for measuring vapor and thermocouples in the cylindrical test piece

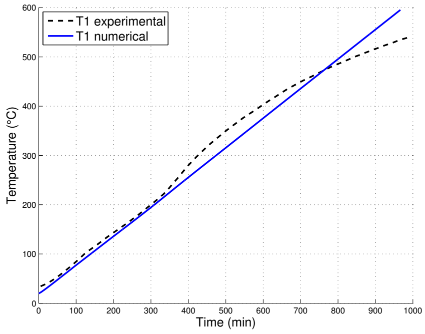

(a) P1

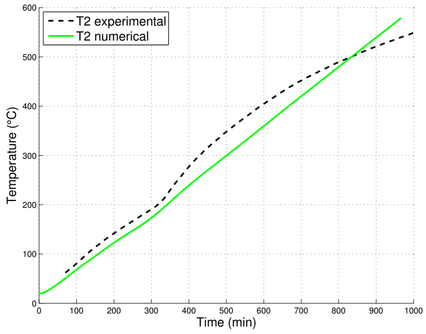

(b) P2

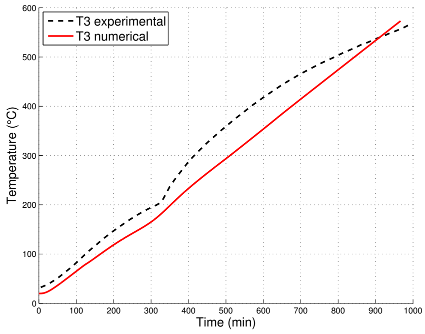

(c) P3

Figure 7: B40 - Temperatures

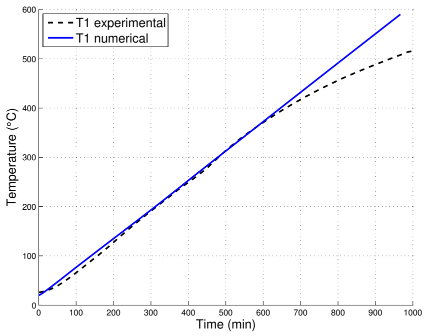

(a) P1

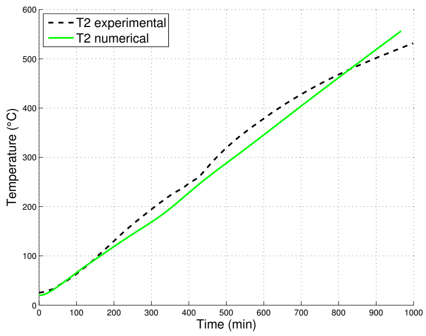

(b) P2

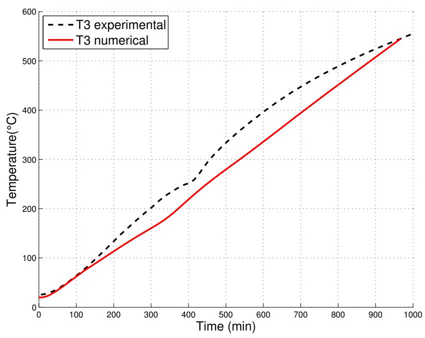

(c) P3

Figure 8: B60 - Temperatures

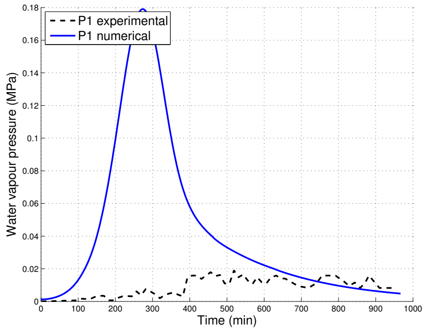

(a) P1

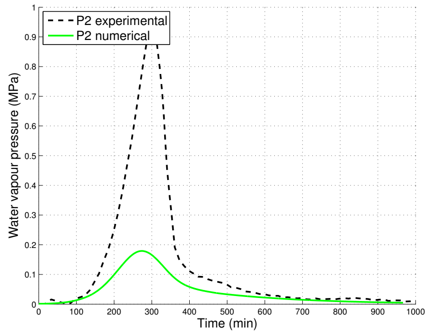

(b) P2

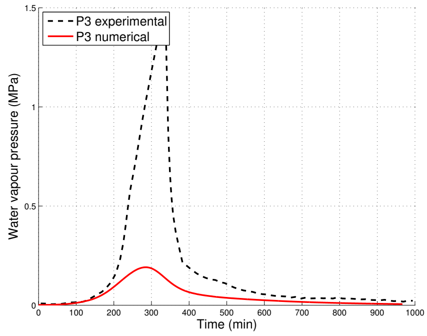

(c) P3

Figure 9: B40 - Water vapor pressure

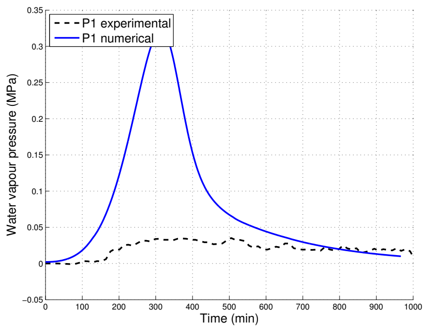

(a) P1

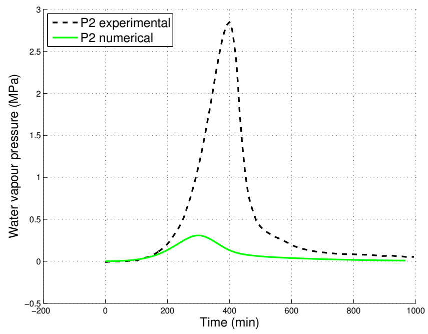

(b) P2

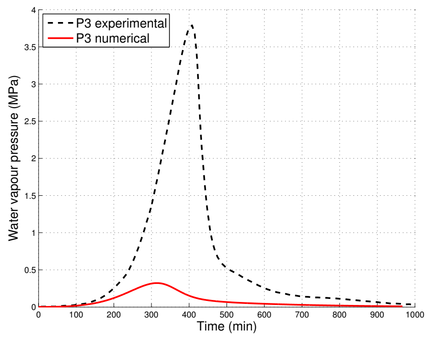

(c) P3

Figure 10: B60 - Water vapor pressure

The water vapor pressure results are shown in Fig. 9 and Fig. 10. For both concrete formulations, $B40$ and $B60$, it is possible to observe that the curve obtained numerically follow the experimental data evolution. However, the numerical values are way smaller than the experimental ones for points $P2$ and $P3$, and for the point $P1$ the numerical values are greater than experimental ones.

7 CONCLUDING REMARKS

This work explored the model proposed by Sercombe *et al.* (2001) and finished at L2MGC by Morais *et al.* (2006a). Relevant concepts for the phenomena were presented. Afterwards, the mathematical model, discretization technique, constitutive equations, and parameters were detailed.

Experimental data relative to concrete was applied to validate the model, tests with different loads, geometries, initial and boundary conditions were used. However, only the one based on Mindeguia (2009) was somehow successful.

In Experiment 1, based on Mounajed & Obeid (2004), the almost nul initial value for relative humidity caused issues, demonstrating that the model is sensible approximately dry material, being incapable of performing analysis in this situation. Experiment 2, based on Ranc *et al.* (2003), present problems relative to the boundary conditions, both thermal and hydric. It is supposed that convection conditions are necessary. Experiment 3, based on Mindeguia (2009), performed without problems, and the temperature responses were adequate. On the other hand, the water vapor pressure results were not what was expected. Even if the shape of the curves were suitable, the results values were not.

In general, it is possible to conclude that the utilization of this model requires a careful calibration of input data, from material parameters and properties, to loads and boundary conditions. When this calibration is well done, the model gives good qualitative results for temperature, mass loss, saturation and water vapor pressure. For the first two, temperature and mass loss, the model was validated in Soares *et al.* (2016), and the results values are as good as the evolution trend. There are saturation responses that exceed this property maximum viable value, as it can be seen in Ferreira *et al.* (2014) and Soares *et al.* (2016). This means that even if the results are qualitatively good, these saturation values imply in the existence of incoherence or limitation to the model. These questions were discussed in Soares *et al.* (2017).

As future works, two distinct approaches are foreseen: explore the inclusion of convection, suggest modifications to the model to solve the problems diagnosed in saturation and water vapor pressure; or propose a new model based on assumptions that do not cause restrictions.

ACKNOWLEDGEMENTS

The authors would like to acknowledge the financial support provided by UFJF, CAPES, FAPEMIG and CNPq.

REFERENCES

Dal Pont, S., 2004. *Lien entre la perméabilité et l'endommagement dans les bétons à haute température*. Ph.D. thesis.

Ferreira, A. P. G., Farage, M. C., Barbosa, F. S., Noumow?, A., & Renault, N., 2014. Thermo-hydric analysis of concrete-rock bilayers under fire conditions. *Engineering Structures*. vol. 59, pp. 765–775.

Kanema, M., Noumowe, A., Gallias, J.-L., & Cabrillac, R., 2005. Influence of the mix parameters and microstructure on the behaviour of concrete at high temperature. In *Proceedings of 18th international conference on structural mechanics in reactor technology*.

Mindeguia, J.-C., 2009. *Contribution exprimentale la comprhension des risques d'instabilit thermique des btons*. Ph.D. thesis. Universit de Pau et des Pays de l'Adour.
URL: *https://hal.archives-ouvertes.fr/tel-00418218/*

Mindeguia, J.-C., Pimienta, P., Noumow, A., & Kanema, M., 2010. Temperature, pore pressure and mass variation of concrete subjected to high temperature Experimental and numerical discussion on spalling risk. *Cement and Concrete Research*. vol. 40, n. 3, pp. 477–487.

Morais, M. V., Bary, B., Durand, S., Ranc, G., & Dal Pont, S., 2007. Numerical analysis of coupled thermo-hydro-mechanical models for concrete exposed to moderate temperatures. In *XXVIII Iberian Latin American Congress on Computational Methods in Engineering (CIL-AMCE 2007). Porto, Portugal*.

Morais, M. V., Pliya, P., Noumow, A., Beaucour, A.-L., & Ortola, S., 2010. Contribution to the explanation of the spalling of small specimen without any mechanical restraint exposed to high temperature. *Nuclear Engineering and Design*. vol. 240, n. 10, pp. 2655–2663.

Morais, M. V. G., Noumowé, A., Kanema, M., Gallias, J.-L., & Cabrillac, R., 2006a. Transferts thermo-hydriques dans un élément en béton exposé à une température élevée: Approches numérique et expérimentale. *24ème Rencontres Universitaires de Génie Civil (AUGC06)*, pp. 1–10.

Morais, M. V. G., Noumow, A., Kanema, M., Gallias, J.-L., & Cabrillac, R., 2006b. Transferts thermo-hydriques dans un élément en béton exposé à une température élevée: Approches numérique et expérimentale. *24me Rencontres Universitaires de Gnie Civil (AUGC06)*, pp. 1–10.

Mounajed, G. & Obeid, W., 2004. A new coupling FE model for the simulation of thermal-hydro-mechanical behaviour of concretes at high temperatures. *Materials and Structures*. vol. 37, n. 6, pp. 422–432.
URL: *http://www.springerlink.com/index/H1UW400063R62698.pdf*

Nguyen, V. T., 2013. *Comportement des bétons ordinaire et à hautes performances soumis à haute température: application à des éprouvettes de grandes dimensions*. Ph.D. thesis. Cergy-Pontoise.

Ranc, G., Sercombe, J., & Rodrigues, S., 2003. Comportement haute temprature du bton de structure: Impact de la fissuration sur les transferts hydriques. *Revue Franaise de Gnie Civil*. vol. 7, n. 4, pp. 397–424.
URL: *http://www.tandfonline.com/doi/abs/10.1080/12795119.2003.9692502*

Sercombe, J., Galle, C., & Ranc, G., 2001. Modélisation du comportement du béton à haute température: Transferts des fluides et de chaleur et déformations pendant les transitoires thermiques. *Note Technique SCCME*. vol. 81.

Soares, R. L. T., CR, M., Bastos, F. S., & Norbert, R., 2017. Modelagem termo-hdrica do comportamento do concreto sob temperaturas elevadas. *Mecánica Computacional*. vol. XXXV, n. 35.

Soares, T. R., Farage, M. C., & Renault, N., 2016. Análise termo-hídrica do concreto utilizando o CASTEM. *Revista Interdisciplinar de Pesquisa em Engenharia - RIPE*. vol. v.2 n.18, pp. 307–324.